DOI: 10.32615/ps.2019.172 PHOTOSYNTHETICA 58 (SI): 358-368, 2020

Special issue in honour of Prof. Reto J. Strasser

Action of alamethicin in photosystem II probed by the fast chlorophyll fluorescence rise kinetics and the JIP-test

W. XIAO[*], H. WANG[*], W. LIU[*], X. WANG[*], Y. GUO[*], R.J. STRASSER[*,**], S. QIANG[*], S. CHEN[*,+], and Z. HU[***]

Weed Research Laboratory, Nanjing Agricultural University, 210095 Nanjing, China[*]
Bioenergetics Laboratory, University of Geneva, CH-1254 Jussy/Geneva, Switzerland[**]
Key Laboratory of Plant Stress Biology, School of Life Sciences, Henan University, 475004 Kaifeng, China[***]

Abstract

Alamethicin (AMT) is a linear antimicrobial peptide isolated from fungi *Trichoderma viride.* To date, the mode of action of AMT in plant cells remains unknown. Our experimental results indicate that AMT causes leaf lesion attributed to its multiple effects on PSII. AMT decreases the O_2 evolution rate of PSII. Based on chlorophyll fluorescence data, similar to the classical herbicide diuron, AMT interrupts PSII electron transfer beyond Q_A at the acceptor side, leading to the inactivation of the PSII reaction centers. Additionally, AMT decreases chlorophyll content and destroys the architecture of PSII pigment assemblies. However, AMT does not affect the oxygen-evolving complex at the donor side of PSII. Thus, it is concluded that AMT is a natural photosynthetic inhibitor with several action sites in PSII.

Additional key words: bioherbicide; chlorophyll *a* fluorescence; leaf lesion; natural product.

Introduction

Alamethicin (AMT), a mycotoxin produced by *Trichoderma viride*, has a linear sequence consisting of 20 amino acid residues with a phenylalaninol at the C-terminus and an acetylated N-terminus (Payne *et al*. 1970, Leitgeb *et al*. 2007; Fig. 1*A*). AMT has a broad range of biological activities by interacting with cell membranes, including cytolytic activity towards mammalian cells, tissue damage in insect larvae, and antimicrobial activity (Meyer and Reusser 1967, Dathe *et al*. 1998, Fehri *et al*. 2007, Thippeswamy *et al*. 2009, Aidemark *et al*. 2010).

AMT is also used in plant physiology research for its cell membrane permeation function and for inducing the plant defense mechanisms. At appropriate concentrations, AMT damages the roots and leaves of *Arabidopsis* and causes rapidly cell death. This is attributed to the inhibition of protein synthesis and rRNA cleavage. The noncoding region of AMT is the main factor inducing rRNA cleavage (Rippa *et al*. 2007). AMT also causes hypersensitive response-(HR-)like cell death and leaf lesions in *Arabidopsis*, being characterized by a significant increase in the expression level of the defense-related genes *PR2* and *PDF1.2*, production of volatile terpenoids, activation of jasmonic acid and salicylic acid defense signals. The response is associated with cell shrinkage and DNA fragmentation (Engelberth *et al*. 2001, Rippa *et al*. 2010, Li *et al*. 2018). Furthermore, AMT changes the permeability of mitochondrial membranes and increases oxygen consumption with NADH in leaf mitochondria (Juszczuk *et al*. 2007). AMT is thought to be able to permeate into the cell walls of *Arabidopsis* and tobacco and induce the synthesis of callose synthase (Aidemark *et al*. 2009). The contact between the plasma membrane and the cell wall may be essential for plants to remain resistance for AMT (Dotson *et al*. 2018). Additionaly, the interaction between AMT and plants may be related to the gated outwardly rectifying K^+ channel proteins (Shi *et al*. 2016). Therefore, AMT has phytotoxic and potential herbicidal activity. However, the detailed mechanism of action of AMT in plant cells is still unclear, particularly because its effect on photosynthesis is poorly understood.

Photosynthesis is the key physicochemical process for plant growth and survival. Photosynthetic activity

Received 28 August 2019, *accepted* 13 December 2019.
[+]Corresponding author; e-mail: chenshg@njau.edu.cn
Abbreviations: ABS – absorption flux; AMT – alamethicin; Chl – chlorophyll; CS – per excited leaf cross section; DCMU – 3-(3,4-dichlorophenyl)-1,1-dimethylurea; DMSO – dimethyl sulfoxide; ETR – electron transport rate; F_V/F_M – maximum quantum yield of PSII photochemistry; OEC – oxygen-evolving complex; q_P – photochemistry quenching coefficient; RCs – reaction centers; ROS – reactive oxygen species; TAP – Tris-acetate-phosphate; TR_0 – trapping flux.
Acknowledgements: This work was supported by the National Key Research and Development Program (2017YFD0201300), the Foreign Expert Project (G20190010118), and the Fundamental Research Funds for the Central Universities (KYZ201530). We also thank Dr. Bernal E. Valverde (Research and Development in Tropical Agriculture, Costa Rica) for improving the language.

can be influenced by several external factors, including CO_2 concentration, light intensity, humidity, temperature, mechanical damage, microbial attack and chemicals (Schwarz *et al*. 1997, Chen *et al*. 2011, Wang *et al*. 2015, Tomimatsu and Tang 2016). The photosynthetic apparatus is regarded as the most major and important target site of herbicide because of its central function in plant mechanism. During the past 30 years, the fast chlorophyll (Chl) fluorescence rise kinentics OJIP, based on the so-called 'Theory of Energy Fluxes in Biomembranes', has been widely used as an excellent tool to probe plant stress physiological states because of its nondestructive, precise, and quick characteristic (Strasser *et al*. 1995, 2004; Chen *et al*. 2016).

Here, the site and mode of action of AMT in PSII was investigated by physiological and biochemical methods, especially fast Chl *a* fluorescence rise kinetics OJIP and JIP-test analysis. Multiple effects of AMT on PSII were identified leading to cell death and leaf lesions in *Arabidopsis*. In *Chlamydomonas reinhardtii* and *Arabidopsis*, AMT acts as a novel natural photosynthetic inhibitor. It can inhibit oxygen evolution of PSII and interrupt PSII electron transport beyond Q_A^-. AMT also damages PSII pigment assemblies and decreases Chl content.

Materials and methods

Plant materials and chemicals: The green alga, *C. reinhardtii*, wild-type strain, was obtained from the Freshwater Algae Culture Collection at the Institute of Hydrobiology (FACHB-Collection, Chinese Academy of Science, China). Cells were grown in Tris-acetate-phosphate (TAP) medium at 25°C under white light of 100 μmol(photon) m^{-2} s^{-1} (day/night, 12/12 h) and shaken once every 12 h. The logarithmic cells (approximately 3-d) were collected and washed twice with distilled water, then resuspended with buffer A (20 mM HEPES-KOH, pH 7.5, 350 mM sucrose, and 2.0 mM $MgCl_2$). The total biomass was determined by optical density of cell suspensions in a spectrophotometer (*UV-1800*, *Shimadzu*, Japan) at 750 nm (A_{750}) and adjusted to 0.65. The cells were used for the subsequent experiments.

Seeds of *Arabidopsis* (Columbia ecotype) after vernalization treatment (3 d at 4°C) were germinated on a mixture of soil and vermiculite (2:1, v/v), soaked with 1/4 strength Hoagland nutrient solution. Plants were grown in a greenhouse at 20–22°C under white light of about 100 μmol(photon) m^{-2} s^{-1} (day/night, 16/8 h) and 80% relative humidity. After three weeks, the leaves of *Arabidopsis* mature plants were collected as experimental samples.

Alamethicin (*CAS No. 27061-78-5*, AMT), diuron [*CAS No. 330-54-1*, DCMU, 3-(3,4-dichlorophenyl)-1,1-dimethylurea] and dimethyl sulfoxide (DMSO) were purchased from *Sigma-Aldrich*. The AMT and DCMU stock solutions were prepared in 100% DMSO and diluted in distilled water as required. The final concentration of DMSO in every experiment was less than 1% (v/v).

Chl *a* fluorescence imaging and phytotoxicity assay: Chl *a* fluorescence imaging was measured by a pulse-modulated *Imaging-PAM M-series* fluorometer (*MAXI-version*, *Heinz Walz GmbH*, Effeltrich, Germany) in three independent experiments (Massacci *et al*. 2008, Gao *et al*. 2018). Before measurement, the samples were placed under the imaging system camera for 0.5-h dark adaptation after focusing of the camera. Images of fluorescence were recorded at 0.25 μmol(photon) m^{-2} s^{-1} measuring light, 110 μmol(photon) m^{-2} s^{-1} actinic light, and 6,000 μmol(photon) m^{-2} s^{-1} saturation pulse light. Four parameters, electron transport rate (ETR), maximal quantum yield of PSII photochemistry (F_V/F_M), photochemistry quenching coefficient (q_P), and maximal fluorescence yield of the dark-adapted state (F_M), were measured directly.

For *C. reinhardtii* cells, 200 μL of suspensions with 1% DMSO (control), AMT (2.5, 5, 10, and 20 μM) were added into the 96-well black microtiter plate, treating for 2.5 h under 100 μmol(photon) m^{-2} s^{-1} white light at 25°C. After the samples were adapted in darkness for 0.5 h, fluorescence imaging was measured.

For *Arabidopsis*, the detached-intact leaves were rinsed with distilled water, blotted with sterile paper, and placed in a culture dish lined with a moistened filter paper. Subsequently, a 20 μL of 1% DMSO (control) or AMT solution (50, 100, 200, 400, and 800 μM) was added on the upper leaf surface, and then incubated for 12, 24, 48, and 72 h at 22°C under approximately100 μmol(photon) m^{-2} s^{-1} white light (day/night, 12/12 h). After the indicated treatment times, the fluorescence imaging and phytotoxicity assay were recorded. Images of visible lesions were taken with a digital camera (*SX11S, Canon*, Japan) and the diameter of leaf lesions was measured using vernier calipers (*ROHS HORM 2002/95/EC*, *Xifeng*, China). The average size was calculated according to the longest and shortest diameters of leaf lesion. Each mean value was obtained from about 15 leaf samples.

PSII oxygen-evolution rate: The rate of PSII oxygen evolution was determined using a Clark type oxygen electrode (*Hansatech Instruments Ltd.*, King's Lynn, UK). Before measurements, AMT and DCMU were added to 2 mL of cell suspensions with a 0.65 A_{750} to make final concentrations as the indicated (0, 10, 25, 50, and 100 μM AMT; or 0, 0.4, 0.8, and 1 μM DCMU), and then the cells were incubated for 3 h in darkness at 25°C. Treated cells containing 45 μg(Chl) were added into the reaction medium. The PSII reaction medium (4.0 mL) contained 50 mM HEPES-KOH buffer (pH 7.6), 4 mM $K_3Fe(CN)_6$, 5 mM NH_4Cl, and 1 mM p-phenylenediamine. The reaction mixture was illuminated with 400 μmol(photon) m^{-2} s^{-1} red light and the rate of O_2 evolution was recorded after 1 min of illumination. The independent experiment was repeated three times.

Chl *a* fluorescence transients OJIP and JIP-test: *Arabidopsis* leaf discs of 7-mm diameter, rinsed with distilled water, were incubated for 0 to 12 h in 1% DMSO (control), 10 μM DCMU or AMT solution (25, 50, 100, 200, 400, 800 μM) in complete darkness at 25°C. The 25 μM AMT was included because leaf discs are more sensitive to AMT than intact leaves. The samples were dark-adapted

for 0.5 h before measurement. The fluorescence transients OJIP curves were measured at room temperature with a Plant Efficiency Analyzer (*Handy PEA* fluorometer, *Hansatech Instruments Ltd*, King's Lynn, Norfolk, UK). There were 30 repetitions for each treatment. Raw fluorescence OJIP transients were transferred with *Handy PEA V1.30* and *BiolyzerHP3* software to a spreadsheet. The following raw data were used: the initial fluorescence F_O [when all reaction centers (RCs) are open], fluorescence intensity at 300 μs (K-step) was denoted as $F_{300\mu s}$, fluorescence intensity F_J is at 2 ms (J-step), fluorescence intensity F_I is at 30 ms (I-step), the maximal fluorescence intensity F_M (when all reaction centers were closed) is equal to F_P. The raw data of each treatment were averaged and analyzed according to the equations of the JIP-test (Strasser *et al*. 2004, 2010; Appendix).

The JIP-test defines the specific (per reaction center, RC) and the phenomenological (per excited cross section, CS) energy fluxes of the absorbed light by the antenna pigments (ABS), the maximum energy trapping (TR_0), the electron transport beyond Q_A^- (ET_0), and dissipation (DI_0). The PSII behavior can be analyzed and quantified by different JIP-test parameters, including RC/CS (the active RCs per CS), TR_0/RC (trapped energy flux per RC), TR_0/CS (trapped energy flux per CS), ABS/CS (absorption flux per CS), ET_0/CS (electron transport flux per CS), DI_0/CS (dissipate energy flux per CS), ABS/RC (absorption flux per RC), ET_0/RC (electron transport flux per RC), DI_0/RC (dissipate energy flux per RC), S_m/t_{Fmax} (average fraction of open RCs of PSII in the time span between 0 to t_{FM}), φ_{Eo} (probability that an absorbed photon leads to electron transport further than Q_A^-), ψ_{Eo} (probability that an absorbed photon leads to reduction of Q_A), PI_{ABS} (performance index on absorption basis) and so on.

In addition, the Q_A^- reducing RCs can be calculated with the following formula (Chen *et al*. 2014):

$$Q_A^- \text{ reducing RCs} = (RC/RC_{reference}) \times (ABS/ABS_{reference}) = = [(RC/CS)_{treatment}/(RC/CS)_{control}] \times [(ABS/CS)_{treatment}/(ABS/CS)_{control}] \quad (1)$$

The parameter R_J, which reflects the relative changes of V_J, offers a measure of the number of the RCs with the Q_B-site filled by PSII inhibitor (Lazár *et al*. 1998, Chen *et al*. 2014):

$$R_J = (V_{J(treatment)} - V_{J(control)})/(1 - V_{J(control)}) = 1 - (\psi_{Eo(treatment)}/\psi_{Eo(control)}) \quad (2)$$

Statistical analysis: One-way analysis of variance (*ANOVA*) was carried out and means were separated by *Duncan*'s LSD at 95% using *SPSS Statistics 20.0*.

Results

Photosynthetic activity: Chl *a* fluorescence is a very sensitive indicator of the effects of stress on photosynthesis. Chl fluorescence imaging techniques allow rapid confirmation of the effects of AMT on photosynthetic activity by monitoring changes in fluorescence parameters. In Fig. 1*B*, color-coded images of F_V/F_M of AMT-treated *C. reinhardtii* cells are shown. As the concentration increased, the F_V/F_M images gradually faded from blue to green. This result is supported by the values of fluorescence parameter F_V/F_M, which was around 60.8% of control at 20 μM AMT treatment (Fig. 1*C*). ETR exhibited a concentration-dependent decrease. The value of ETR already decreased to 0 at the highest concentration of 20 μM AMT (Fig. 1*D*). It is clear that AMT can affect photosynthetic activity of *C. reinhardtii* largely due to the inhibition of PSII electron transport.

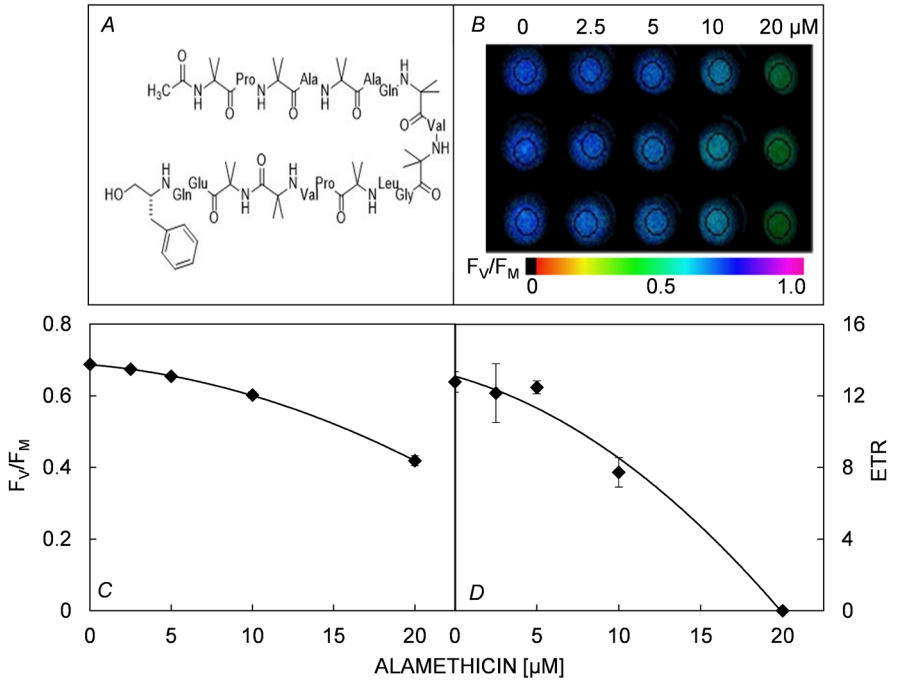

Fig. 1. The chemical structure of alamethicin (AMT) (*A*). Effect of AMT on color fluorescence imaging (*B*), the value of the maximum quantum yield of PSII (F_V/F_M) (*C*), and electron transport rate (ETR) (*D*) of *Chlamydomonas reinhardtii* cells. Fluorescence images were indicated by color code in the order of black (0) through red, orange, yellow, green, blue, violet to purple (1). The number codes above images are marked from 0 to 1, showing the changes. Each value is the average ± SE of three independent experiments with around 15 repetitions.

Rate of PSII oxygen evolution: A substantial decrease of about 63% in the O_2 evolution rate was observed when *C. reinhardtii* cells were exposed to 100 µM AMT for 3 h (Fig 2). AMT had a concentration-dependent negative impact on the O_2 evolution rate. DCMU entirely inhibited O_2 evolution at 1 µM. Therefore, AMT apparently is a weaker PSII inhibitor than DCMU that is a specific PSII inhibitor.

Phytotoxicity of AMT to *Arabidopsis*: In order to further estimate the phytotoxicity of AMT to higher plants, a lesion formation in *Arabidopsis* mature leaves was monitored after AMT treatment with various concentrations (Fig. 3). At the highest concentration of 800 µM, visible leaf lesion began being noticeable after 24 h of treatment, further developing and becoming chlorotic with time. At specific times, leaf lesion size increased in a concentration-dependent manner (Fig. 3*B*). At 72 h of 800 µM AMT treatment, the leaf lesion diameter reached 6.6 mm. Clearly, AMT causes leaf chlorotic lesions. Such symptom confirms that AMT impairs the photosynthetic activity of *Arabidopsis* leaf.

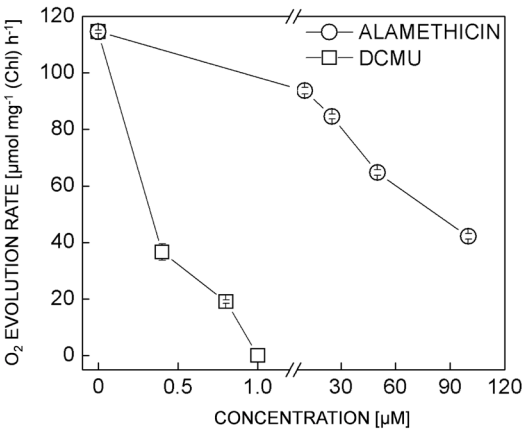

Fig. 2. Effect of alamethicin (AMT) and DCMU on the rate of O_2 evolution of *Chlamydomonas reinhardtii* cells. H_2O and p-phenylenediamine is the electron donor and acceptor, respectively. Data shown are mean values ± SE of three independent measurements with around 15 repetitions.

The damage to *Arabidopsis* leaves was also assessed by fluorescence imaging after AMT treatment. The color-coded images of F_V/F_M gradually changed from blue in the control to black at the highest concentration after different treatment times. These results on physiological damage were well in agreement with the leaf lesions developed by treated plants. The results are strongly supported by the values of fluorescence parameters F_M, F_V/F_M, q_P, and ETR (Fig. 4*B–E*). After 48 h of AMT treatment, the values of F_M and q_P showed a rapid concentration-dependent decrease. However, the ratio of F_V/F_M and the values of ETR decreased much slower than those of C. *reinhardtii*. At 48 h of 800 µM AMT treatment, the value of F_M, q_P, F_V/F_M, and ETR decreased by about 81, 100, 48, and 42% by comparison with control, respectively. q_P shows an approximately linear lowering at different concentrations of AMT. q_P denotes the proportion of excitons captured by open traps and being concerted to chemical energy in the PSII reaction center (Krause and Weis 1991). In summary, AMT affects photosynthesis in *Arabidopsis* mainly by impairing PSII photochemistry.

Fast Chl *a* fluorescence rise kinetics: To further probe the site of action of AMT in PSII, the fluorescence rise kinetics OJIP curves of *Arabidopsis* leaves were measured. The fluorescence rise transients curve of the control exhibited a typical polyphasic O-J-I-P shape (Fig. 5*A*). In the case of AMT and DCMU, remarkable change of the shape of the fluorescence rise transients OJIP curves of *Arabidopsis* leaves already took place. For DCMU, the biggest change was that the J-step increased quickly equal to P level (F_M), which contributes to the large accumulation of Q_A^- in PSII RCs due to blocking the electron flow beyond Q_A (Strasser *et al*. 2004). For AMT, a gradual rise of J-step level and a significant reduction of F_M were observed by increasing treatment concentrations (Fig. 5*A*). At 800 µM AMT, the F_J was so close to its maximum value of F_M that the J became the dominant step of the fluorescence kinetics OJIP (Fig. 5*A*). At 25 µM AMT treatment, the fluorescence

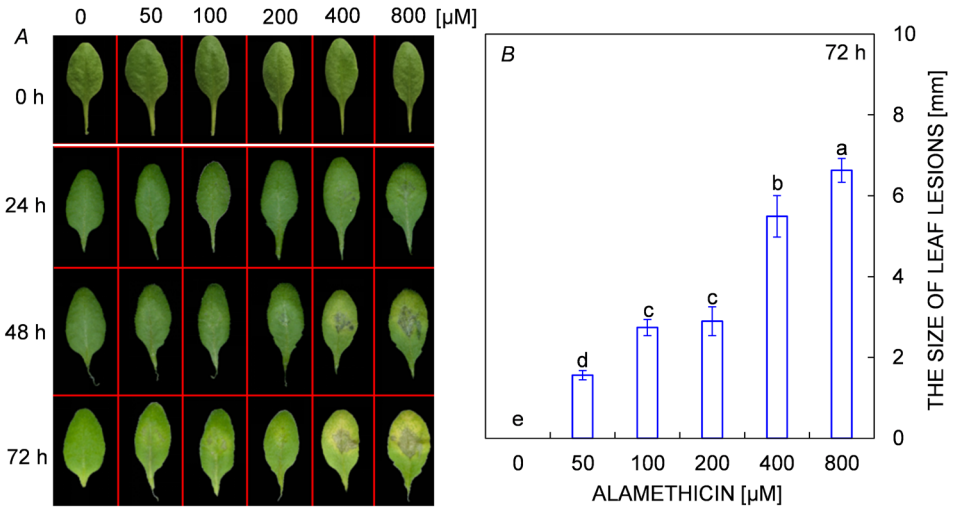

Fig. 3. Leaf lesion formation of the detached-intact *Arabidopsis* leaves after alamethicin (AMT) treatment. Leaves were treated with 1% DMSO (control) or AMT at various concentrations (50, 100, 200, 400, and 800 µM) for 0, 24, 48, and 72 h (*A*). The size of leaf lesion after 72 h of AMT treatment (*B*). Similar results were repeated three times with at least five leaves per each experiment.

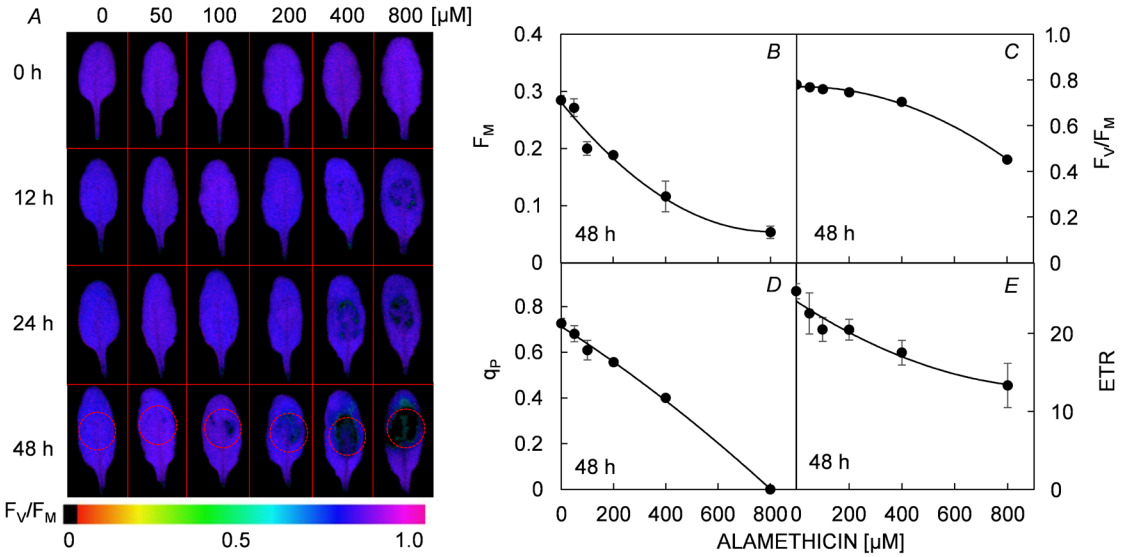

Fig. 4. Color fluorescence imaging of *Arabidopsis* leaves after alamethicin (AMT) treatment (*A*). Effect on the maximal fluorescence (F_M) (*B*), the value of the maximum quantum yield of PSII (F_V/F_M) (*C*), photochemical quenching coefficient (q_P) (*D*), and electron transport rate (ETR) (*E*) of *Arabidopsis* intact leaves after 48 h treatment with different concentrations of AMT (50, 100, 200, 400, and 800 μM). The data of F_M, F_V/F_M, q_P, and ETR were derived from the red circle area of leaf fluorescence images in Fig. 4*A*. Fluorescence images were indicated by color code in the order of black (0) through red, orange, yellow, green, blue, violet to purple (1). The number codes above images are marked from 0 to 1, showing the changes. Each value is the average ± SE of three independent experiments with at least 15 repetitions.

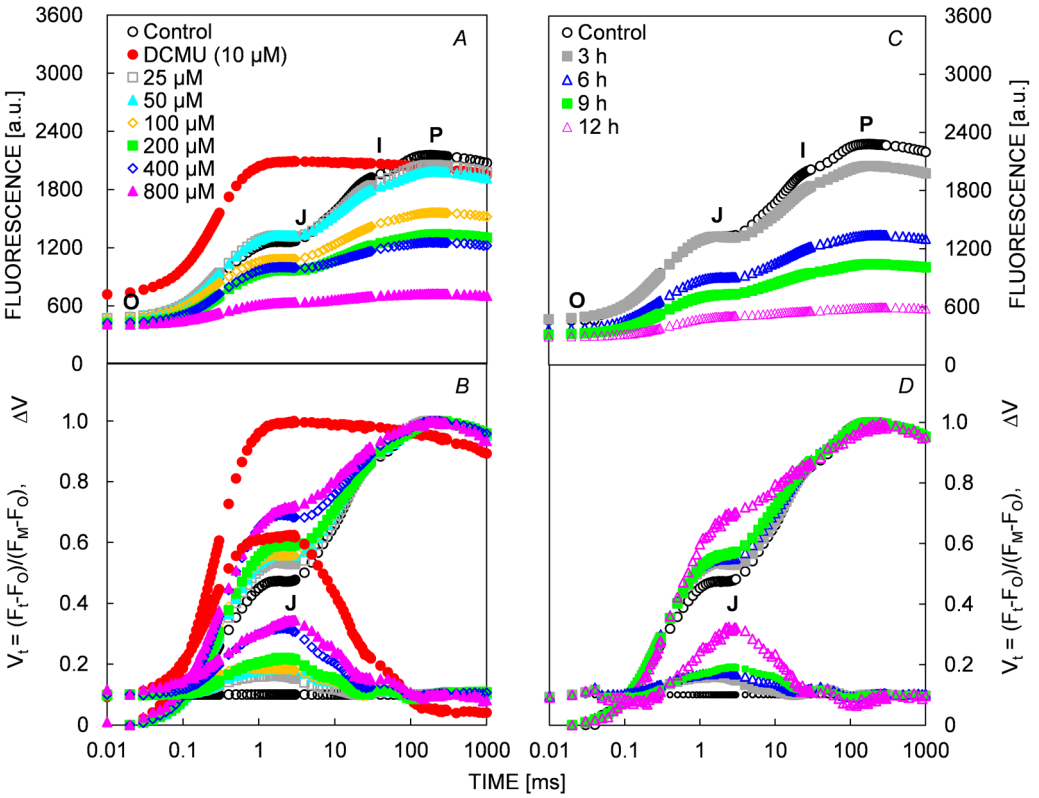

Fig. 5. Chl *a* fluorescence rise kinetics OJIP curves of *Arabidopsis* leaves treated with 1% DMSO (control) or with alamethicin (AMT) at the indicated concentrations and times. After 3 h treatment of AMT with different concentration, raw fluorescence rise kinetics OJIP (*A*), the relative variable fluorescence normalized by F_O and F_M as $V_t = (F_t - F_O)/(F_M - F_O)$ (*top*) and $\Delta V_t = V_{t(treated)} - V_{t(control)}$ (*bottom*) (*B*). After 25 μM AMT treatment for different time, raw fluorescence rise kinetics OJIP (*C*), the relative variable fluorescence normalized by F_O and F_M as $V_t = (F_t - F_O)/(F_M - F_O)$ (*top*) and $\Delta V_t = V_{t(treated)} - V_{t(control)}$ (*bottom*) (*D*). Each value is the average of 30 measurements.

rise transients OJIP curves also exhibited a time-dependent change by increasing treatment time, especially an obvious J-step rise (Fig. 5*C*). The fluorescence data normalized by F_O (the step O, 20 μs) and F_M, as relative variable fluorescence $V_t = (F_t - F_O)/(F_M - F_O)$ and $\triangle V = V_{t(treated)} - V_{t(control)}$, are presented in Fig. 5*B–D*. A significant rise in the J-step level is the major effect of AMT on the fluorescence rise kinetics OJIP curve. This means that AMT inhibits the electron transport at the acceptor side of PSII, resulting in a fast increase of reduced Q_A concentration.

The JIP-test: The fluorescence rise kinetics OJIP is rich in information. Its quantitative analysis can be carried out by the JIP-test. Some selected structural and functional JIP-test parameters can be used to quantify the PSII behavior. The patterns of the selected JIP-test parameters of AMT-treated samples exhibit the similar change at the different treatment – concentration and time (Fig. 6). V_K (the relative variable fluorescence at the K-step) and V_J (the relative variable fluorescence at the J-step) increased with AMT concentration (Fig. 6*A*). At 3 h of exposure to 800 μM AMT, V_J and V_K increased by around 52 and 40%, respectively, relative to the untreated control. However, the values of V_I (the relative variable fluorescence at the I-step) and F_K/F_J remained constant. No effect of AMT on F_K/F_J means an increase of the K-step level resulted from an increase of the J-step level. Our data also suggest that AMT does not affect significantly the oxygen-evolving complex (OEC) centers (*see* Tables 1S, 2S, *supplement*).

The parameters ABS/CS_m, TR_0/CS_m, ET_0/CS_m, RC/CS_m, Q_A-reducing centers, S_m/t_{Fmax}, φ_{Eo}, φ_{Po}, ψ_{Eo}, and PI_{ABS} significantly decreased after AMT treatment (Fig. 6, Tables 1S, 2S). ABS/RC (absorption flux per RC) exhibited somewhat increase at AMT treatment, especially at concentrations above 100 μM. The ABS/RC value increased by 74.0% compared with that of the control at the highest concentration of 800 μM (Fig. 6*A*); however, it remained unchanged at 25 μM treatment despite treatment time (Fig. 6*B*).

Among these parameters, AMT led to a distinct decrease in PSII electron transport efficiency, including φ_{Eo} (the quantum yield for PSII electron transport), ψ_{Eo} (the probability that a trapped exciton moves an electron into the electron transport chain beyond Q_A), and ET_0/CS_m (electron transport flux per excited leaf cross section). At 3 h of 800 μM AMT treatment, φ_{Eo}, ψ_{Eo}, and ET_0/CS_m decreased by about 70, 44, and 92% relative to the control, respectively. At 12 h of 25 μM AMT treatment, φ_{Eo}, ψ_{Eo}, and ET_0/CS_m decreased by about 46, 30, and 82% relative to the control, respectively.

Incubation of *Arabidopsis* leaves with AMT at different concentrations and times decreased the density of the active PSII RCs (RC/CS). At 3 h of 800 μM AMT or 12 h of 25 μM AMT, RC/CS_m was just 16 and 25% of the control, respectively. S_m/t_{Fmax}, expressing the average fraction of open reaction centers of PSII, decreased gradually by increasing concentration or time of AMT treatment. At 3 h of 800 μM AMT or 12 h of 25 μM AMT, S_m/t_{Fmax} was about 59 and 61% of those of the control. The amount of Q_A-reducing centers deceased by 39, 42, 71, 76, 79, and 96% compared with the control, respectively, after 3-h treatment of AMT at 25, 50, 100, 200, 400, and 800 μM.

The PSII performance index on absorption basis, PI_{ABS}, decreased in strong relationship with concentration and time of treatment with AMT (Fig. 6). PI_{ABS} is a product of the three independent components φ_{Po}, ψ_{Eo}, and γ_{RC}. Here, γ_{RC} is the fraction of RC chlorophyll in relation to total chlorophyll (Strasser *et al*. 2004; Appendix). φ_{Po}, reflecting the maximum quantum yield for PSII primary photochemistry, significantly decreased at the high concentrations (400 and 800 μM) or the longest treatment time (12 h). However, no obvious change was

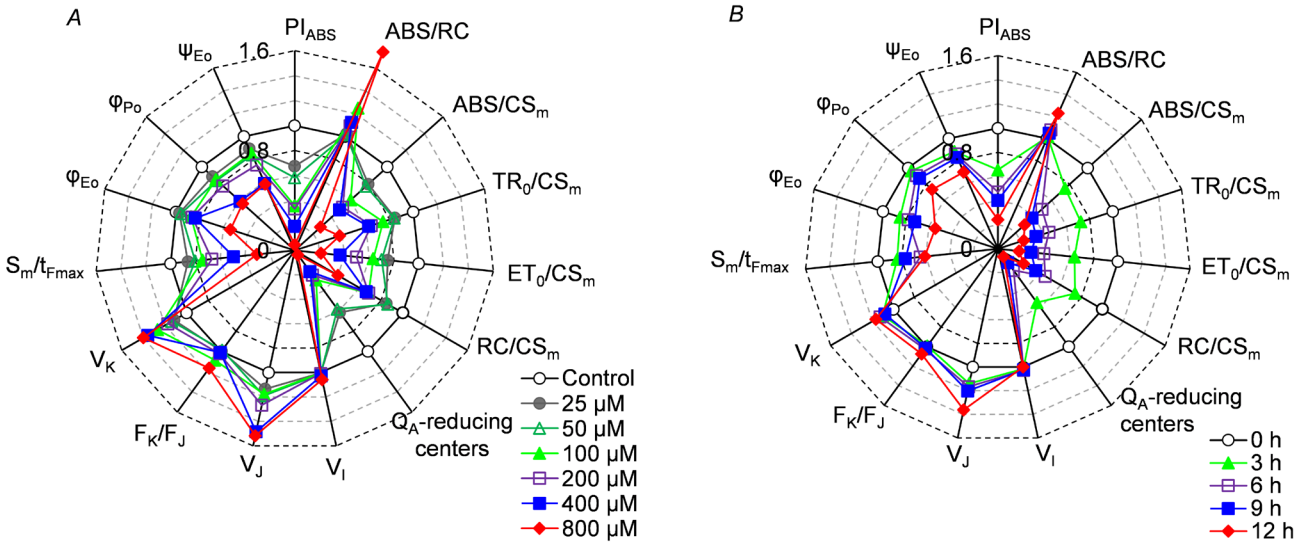

Fig. 6. Radar plot presentation of selected parameters derived from JIP-test quantifying PSII behavior of *Arabidopsis* leaves treated with alamethicin (AMT) with different concentrations for 3 h (*A*) or with 25 μM AMT for different time (*B*). Each parameter is expressed as fraction relatively to the values of the control (back regular circle with value 100% = 1). The original data of these parameters are shown in Tables 1S, 2S.

observed at the low concentrations below 400 μM. To further analyze the contribution of PSII electron transport and chlorophyll content to PI_{ABS}, the relationship between PI_{ABS} and φ_{Eo}, ABS/CS_m or ET_0/CS_m is presented in Fig. 7*A*. The high linear correlation between PI_{ABS} and ABS/CS_m, φ_{Eo} and ET_0/CS_m indicates that the loss of PSII overall photosynthetic activity is mainly attributed to damage of antenna pigment assemblies and inhibition of PSII electron transport efficiency.

To study the binding of AMT to the Q_B-site of the PSII RCs, R_J was introduced to estimate the number of PSII RCs with their Q_B-site filled by AMT. R_J increased with AMT concentration (Fig. 7*B*). After *Arabidopsis* leaves were treated with AMT for 3 h, the amount of PSII RCs with Q_B-site filled by AMT was about 11% (25 μM), 16% (50 μM), 19% (100 μM), 23% (200 μM), 41% (400 μM), and 44% (800 μM), respectively. There is a visible concentration-dependent enhancement of AMT bound to the PSII RCs. A highly negative correlation between R_J and φ_{Eo} or Q_A-reducing centers was observed in the presence of AMT (Fig. 7*C*,*D*). This suggests that AMT-caused severe inactivation of Q_A-reducing centers and inhibition of PSII electron transport is due to the increased number of PSII RCs with the Q_B-site filled with AMT.

Finally, AMT-induced changes in the derived parameters can also be visualized by means of the energy pipeline model of the photosynthetic apparatus. Variation of the value of parameters is expressed by the different width of the corresponding arrow. Two types of models are shown, including the membrane model and leaf model (Fig. 8). With the increasing of AMT treatment concentration, the absorption flux per RC (ABS/RC) and dissipated energy flux per RC (DI_0/RC) clearly increased (left side of Fig. 8). The electron transport flux per RC or CS (ET_0/RC or ET_0/CS_m), absorption and trapping flux per excited CS (ABS/CS_m and TR_0/CS_m), and amount of active PSII RCs declined significantly. It is notable that AMT treatment resulted in a gradual loss of green color of leaf in the leaf model (right side of Fig. 8). Thus the action mechanism of AMT is the inactivation of PSII RCs caused by the blocking PSII electron transport at the acceptor side, and damage to pigment assemblies (ABS/CS_m or TR_0/CS_m).

Discussion

Rippa *et al*. (2010) reported that AMT can cause HR-like cell death of *Arabidopsis* leaves. AMT causes cell death of *Arabidopsis* leaves as signed by foliar yellow lesions (Fig. 3). Such chlorotic or necrotic symptoms indicate that AMT damages photosynthetic tissues. Evidence from fluorescence imaging suggest that AMT decreases significantly the maximal quantum yield of PSII (F_V/F_M), electron transport rate (ETR), and photochemistry quenching coefficient (q_P) (Fig. 1*B–D*, Fig. 4). The F_V/F_M ratio is an important and easily measurable parameter of the physiological state of the photosynthetic apparatus. ETR represents the apparent photosynthetic electron transport. q_P denotes the proportion of excitons captured by open traps and being converted to chemical energy in the PSII reaction center (Krause and Weis 1991). The value of q_P depends on the presence of Q_A in the oxidized state. The strong decrease of q_P suggests the loss of PSII photosynthetic activity by affecting the efficiency of the overall photochemical process and the functional state of PSII. In the presence of AMT, the rate of oxygen evolution of PSII of *C. reinhardtii* exhibits a concentration-dependent decrease. This indicates that the PSII is the important

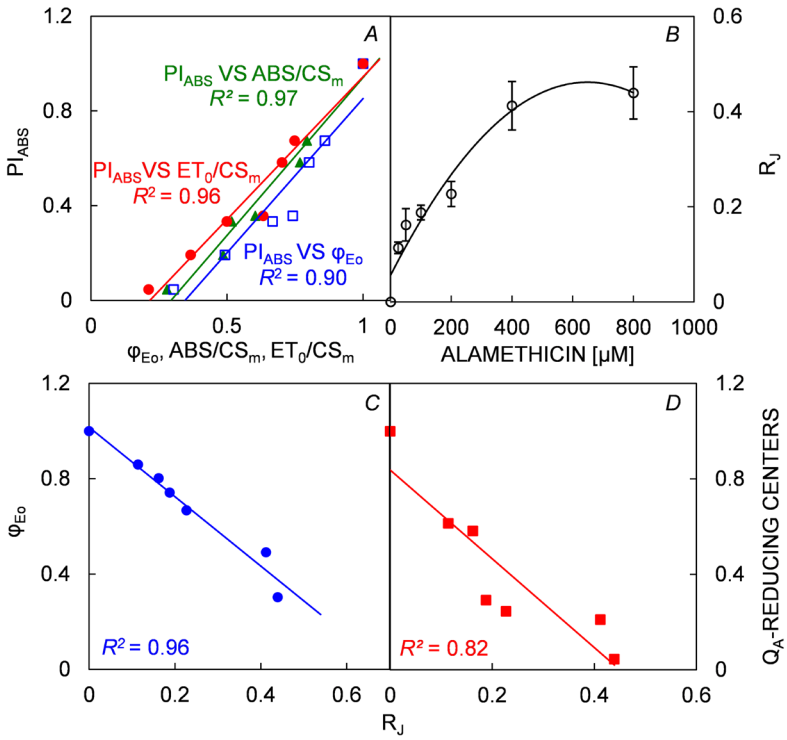

Fig. 7. Analysis of the linear relationship between JIP-test parameter PI_{ABS} (the performance index on absorption basis) and ET_0/CS (electron transport flux per CS), ABS/CS_m (absorption flux per excited CS), or φ_{Eo} (quantum yield for electron transport) after *Arabidopsis* leaves were treated with alamethicin (AMT) (*A*). The concentration-dependent change of R_J (the number of PSII RCs with Q_B-site filled by PSII inhibitor) (*B*). The parameter R_J reflects the number of PSII RCs with their Q_B site filled by PSII inhibitors (here is AMT). Analysis of the linear relationship between R_J and φ_{Eo} (*C*) or Q_A-reducing centers (*D*). Each value is the average of 30 measurements.

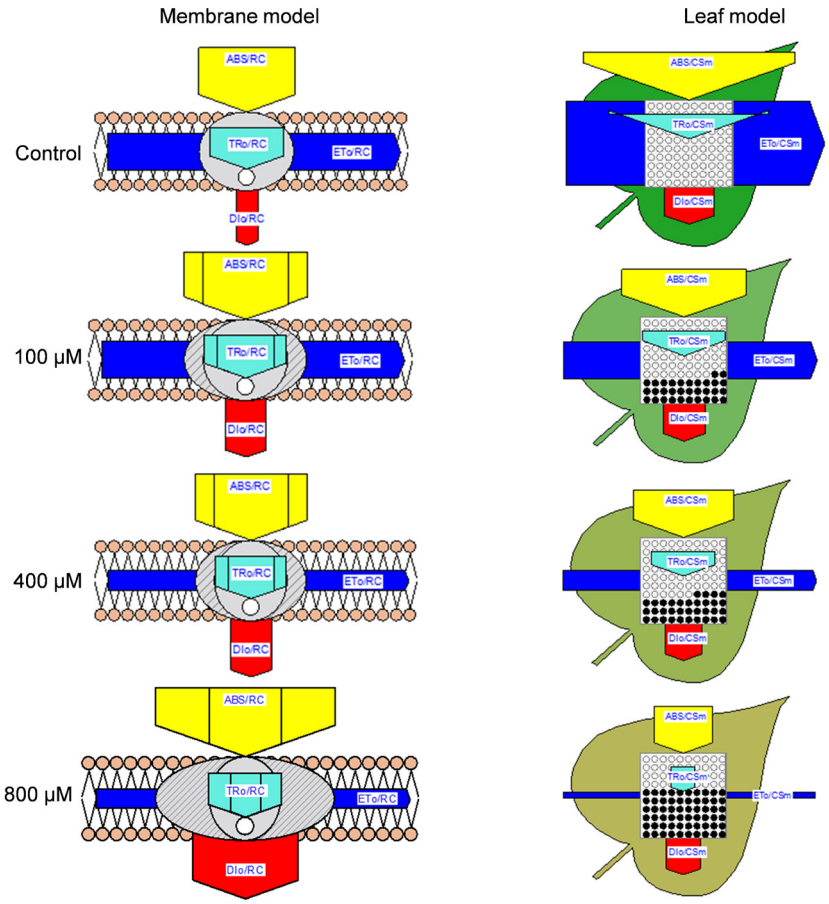

Fig. 8. Pipeline models showing relative changes in energy flows per reaction center (*left panel*) and per active leaf cross section (*right panel*) after 100, 400, and 800 µM alamethicin (AMT) treatment of an *Arabidopsis* leaf. The response of each of parameters can be seen in the relative change in the width of each arrow relative to the control sample (1% DMSO). Active RCs are shown as *open circles* and inactive RC_S are as *filled black circles*.

action target of AMT.

To further identify and localize the action site of AMT in PSII, the fast fluorescence rise kinetics OJIP and the JIP-test are used. Firstly, AMT does not affect the K-step level (Fig. 6). Occurrence of the K-step is related to the inactivation of the OEC leading to an imbalance between the electron flow leaving the RC towards the acceptor side and the electron flow coming to the RC from the donor side of PSII (Strasser *et al*. 2004). This indicates that AMT has no effect on OEC. A rapid rise of the J-step level is the greatest change of the fluorescence rise kinetics OJIP curves of AMT-treated *Arabidopsis* leaves (Figs. 5, 6), which can be attributed to a large accumulation of Q_A^- after the interruption of the electron flow beyond Q_A at the acceptor side of PSII (Strasser *et al*. 2004). This is corroborated by all ET-related parameters. In the presence of AMT, ET_0/CS_m, φ_{Eo}, and ψ_{Eo} significantly decreased (Fig. 6). Since AMT inhibits electron transfer beyond Q_A at the acceptor side of PSII, inactivation events are also expected at PSII RCs. The number of active PSII RCs per cross section (RC/CS_m), and the average fraction of open RCs of PSII (S_m/t_{Fmax}) decline quickly after AMT treatment (Fig. 6), implying a likely severe closure of PSII RCs. The fraction of Q_A-reducing centers can be calculated according to Chen *et al*. (2014). A dramatic concentration-dependent decrease in Q_A-reducing centers was found after AMT treatment (Fig. 6*A*). It is interesting that the decrease of Q_A-reducing centers is much more than that of ET_0/CS_m, φ_{Eo}, and ψ_{Eo}. This suggests that factors other than the interruption of electron flow beyond Q_A also contribute to the inactivation of PSII RCs. In contrast with Q_A-reducing centers, AMT increases the proportion of non-Q_A-reducing represented by closed black circles increased in the leaf model (Fig. 8). Non-Q_A-reducing centers, also so-called heat sink centers, are radiators and often are used to protect the system from over excitation and over reduction which would produce dangerous ROS (Strasser *et al*. 2004, Chen *et al*. 2014). It is assumed that ROS production may be indirectly responsible for the inactivation of PSII RCs.

The distinct decrease in the P level (F_M) observed in the fluorescence rise OJIP curves of AMT-treated leaves (Fig. 5*A*,*C*) might be associated with the quenching of fluorescence, which resulted from the presence of an oxidized plastoquinone pool or the damage of the structure and function of PSII antennae (Tóth *et al*. 2005). ABS/CS_m expresses the total absorption flux per active leaf cross section, and can be taken as a measure for an average antenna size or Chl concentration (Srivastava *et al*. 1998, Strasser *et al*. 2004). TR_0/CS_m refers to the trapped energy flux per active leaf cross section, reflecting the specific rate of the exciton trapped by open RCs from the antenna pigment molecules (Strasser *et al*. 2004). A visible time- and concentration-dependent decrease in ABS/CS_m indicates that AMT reduces the Chl concentration (Fig. 6). A significant decrease of TR_0/CS_m demonstrates that AMT destroys the conformation of the antenna pigment

assemblies and decreases the efficiency of light energy transfer between antenna pigment molecules and from those to the PSII RCs. This may also explain the decrease of the F_M value. However, ABS/RC as average antenna size per RC increased at high AMT concentrations that inactivated PSII RCs.

The performance index, PI_{ABS}, reflecting the overall photosynthetic activity of PSII, is the most sensitive experimentally derived parameter to various stress conditions (Strasser *et al*. 2004). AMT has concentration- and time-dependent inhibitory effect on PI_{ABS} (Fig. 6). There is a linear relationship between PI_{ABS} and ET_0/CS_m or φ_{Eo}, and ABS/CS_m, in AMT-treated leaves (Fig. 7*A*). This further proves that AMT inhibits the overall photosynthetic activity of PSII by destroying pigment assemblies and inactivating RCs after blocking electron transfer beyond Q_A at the acceptor side. The parameter R_J has been used to represent the number of PSII RCs with Q_B-site filled by PSII inhibitors (Lazár *et al*. 1998, Chen *et al*. 2014). Thus, a concentration-dependent increase in R_J indicates AMT binds to the PSII RCs (Fig. 7*B*). According to the highly negative correlation between R_J and φ_{Eo} or Q_A-reducing centers (Fig. 7*C*,*D*), the inactivation of PSII RCs caused by AMT mainly results from an enhancement of the number of PSII RCs with the Q_B-site filled by the compound. Thus, the PSII RCs with the Q_B-site may be one of the primary action sites of AMT.

In summary, we posit that AMT causes leaf lesion due to the loss of PSII overall photosynthetic activity. First, AMT strongly inhibits the rate of O_2 evolution and electron transport at the acceptor side of PSII. The main action of AMT is blocking electron flow beyond Q_A, then inactivating the PSII RC_S. Second, AMT decreases the chlorophyll content and destroys the conformation of the antenna pigment assemblies. Such multiple effects lead to damage to the structure and function of PSII.

References

Aidemark M., Andersson C.J., Rasmusson A.G., Widell S.: Regulation of callose synthase activity *in situ* in alamethicin-permeabilized *Arabidopsis* and tobacco suspension cells. – BMC Plant Biol. **9**: 27, 2009.

Aidemark M., Tjellström H., Sandelius A.S. *et al*.: *Trichoderma viride* cellulase induces resistance to the antibiotic pore-forming peptide alamethicin associated with changes in the plasma membrane lipid composition of tobacco BY-2 cells. – BMC Plant Biol. **10**: 274, 2010.

Chen S., Strasser R.J., Qiang S.: *In vivo* assessment of effect of phytotoxin tenuazonic acid on PSII reaction centers. – Plant Physiol. Bioch. **84**: 10-21, 2014.

Chen S., Yang J., Zhang M. *et al.*: Classification and characteristics of heat tolerance in *Ageratina adenophora* populations using fast chlorophyll *a* fluorescence rise O-J-I-P. – Environ. Exp. Bot. **122**: 126-140, 2016.

Chen S., Zhou F., Yin C. *et al*.: Application of fast chlorophyll *a* fluorescence kinetics to probe action target of 3-acetyl-5-isopropyltetramic acid. – Environ. Exp. Bot. **71**: 269-279, 2011.

Dathe M., Kaduk C., Tachikawa E. *et al*.: Proline at position 14 of alamethicin is essential for hemolytic activity, catecholamine secretion from chromaffin cells and enhanced metabolic activity in endothelial cells. – BBA-Biomembranes **1370**: 175-183, 1998.

Dotson B.R., Soltan D., Schmidt J. *et al*.: The antibiotic peptaibol alamethicin from *Trichoderma* permeabilises *Arabidopsis* root apical meristem and epidermis but is antagonised by cellulase-induced resistance to alamethicin. – BMC Plant Biol. **18**: 165, 2018.

Engelberth J., Koch T., Schüler G.: Ion channel-forming alamethicin is a potent elicitor of volatile biosynthesis and tendril coiling. Cross talk between jasmonate and salicylate signaling in lima bean. – Plant Physiol. **125**: 369-377, 2001.

Fehri L.F., Wróblewski H., Blanchard A.: Activities of antimicrobial peptides and synergy with enrofloxacin against *Mycoplasma pulmonis*. – Antimicrob. Agents Ch. **51**: 468-474, 2007.

Gao Y., Liu W., Wang X. *et al*.: Comparative phytotoxicity of usnic acid, salicylic acid, cinnamic acid and benzoic acid on photosynthetic apparatus of *Chlamydomonas reinhardtii*. – Plant Physiol. Bioch. **128**: 1-12, 2018.

Juszczuk I.M., Flexas J., Szal B. *et al*.: Effect of mitochondrial genome rearrangement on respiratory activity, photosynthesis, photorespiration and energy status of MSC16 cucumber (*Cucumis sativus*) mutant. – Physiol. Plantarum **131**: 527-541, 2007.

Krause G.H., Weis E.: Chlorophyll fluorescence and photosynthesis: The basics. – Annu. Rev. Plant Phys. **42**: 313-349, 1991.

Lazár D., Brokeš M., Nauš J., Dvořák L.: Mathematical modeling of 3-(3',4'-dichlorophenyl)-1,1-dimethylurea action in plant leaves. – J. Theor. Biol. **191**: 79-86, 1998.

Leitgeb B., Szekeres A., Manczinger L. *et al*.: The history of alamethicin: A review of the most extensively studied peptaibol. – Chem. Biodivers. **4**: 1027-1051, 2007.

Li F., Li W., Lin Y. *et al*.: Expression of lima bean terpene synthases in rice enhances recruitment of a beneficial enemy of a major rice pest. – Plant Cell Environ. **41**: 111-120, 2018.

Massacci A., Nabiev S.M., Pietrosanti L. *et al*.: Response of the photosynthetic apparatus of cotton (*Gossypium hirsutum*) to the onset of drought stress under field conditions studied by gas-exchange analysis and chlorophyll fluorescence imaging. – Plant Physiol. Bioch. **46**: 189-195, 2008.

Meyer C.E., Reusser F.: A polypeptide antibacterial agent isolated from *Trichoderma viride*. – Experientia **23**: 85-86, 1967.

Payne J.W., Jakes R., Hartley B.S.: The primary structure of alamethicin. – Biochem. J. **117**: 757-766, 1970.

Rippa S., Adenier H., Derbaly M., Béven L.: The peptaibol alamethicin induces an rRNA-cleavage-associated death in *Arabidopsis thaliana.* – Chem. Biodivers. **4**: 1360-1373, 2007.

Rippa S., Eid M., Formaggio F. *et al*.: Hypersensitive-like response to the pore-former peptaibol alamethicin in *Arabidopsis thaliana*. – Chembiochem. **11**: 2042-2049, 2010.

Schwarz P.A, Fahey T.J, Dawson T.E.: Seasonal air and soil temperature effects on photosynthesis in red spruce (*Picea rubens*) saplings. – Tree Physiol. **17**: 187-194, 1997.

Shi W., Chen X., Wang L. *et al*.: Cellular and molecular insight into the inhibition of primary root growth of *Arabidopsis* induced by peptaibols, a class of linear peptide antibiotics mainly produced by *Trichoderma* spp. – J. Exp. Bot. **67**: 2191-2205, 2016.

Srivastava A., Jüttner F., Strasser R.J.: Action of the allelochemical, fischerellin A, on photosystem II. – BBA-Bioenergetics **1364**: 326-336, 1998.

Strasser R.J., Srivastava A., Govindjee: Polyphasic chlorophyll *a* fluorescence transient in plants and cyanobacteria. – J. Photoch. Photobio. B **61**: 32-42, 1995.

Strasser R.J., Tsimilli-Michael M., Qiang S., Goltsev V.: Simultaneous *in vivo* recording of prompt and delayed fluorescence and 820-nm reflection changes during drying and after rehydration of the resurrection plant *Haberlea rhodopensis*. – BBA-Bioenergetics **1797**: 1313-1326, 2010.

Strasser R.J., Tsimilli-Michael M., Srivastava A.: Analysis of the chlorophyll *a* fluorescence transient. – In: Papageorgiou G.C., Govindjee (ed.): Chlorophyll *a* Fluorescence: A Signature of Photosynthesis. Advances in Photosynthesis and Respiration. Pp. 321-362. Springer, Dordrecht 2004.

Thippeswamy H.S., Sood S.K., Venkateswarlu R., Raj I.: Membranes of five-fold alamethicin-resistant *Staphylococcus aureus*, *Enterococcus faecalis* and *Bacillus cereus* show decreased interactions with alamethicin due to changes in membrane fluidity and surface charge. – Ann. Microbiol. **59**: 593, 2009.

Tomimatsu H., Tang Y.H.: Effects of high CO_2 levels on dynamic photosynthesis: carbon gain, mechanisms, and environmental interactions. – J. Plant Res. **129**: 365-377, 2016.

Tóth S.Z., Schansker G., Strasser R.J.: In intact leaves, the maximum fluorescence level (F_M) is independent of the redox state of the plastoquinone pool: a DCMU-inhibition study. – BBA-Bioenergetics **1708**: 275-282, 2005.

Wang M., Xie B., Fu Y. *et al.*: Effects of different elevated CO_2 concentrations on chlorophyll contents, gas exchange, water use efficiency, and PSII activity on C_3 and C_4 cereal crops in a closed artificial ecosystem. – Photosynth. Res. **126**: 351-362, 2015.

Appendix. Formula and explanation of the technical data of the OJIP curves and the selected JIP-test parameters used in this study. Subscript '0' (or 'o' when written after another subscript) indicates that the parameter refers to the onset of illumination, when all RCs are assumed to be open.

Technical fluorescence parameters	
F_t	fluorescence at time t after onset of actinic illumination
$F_O \cong F_{20\mu s}$	minimal fluorescence, when all PSII RCs are open
$F_L \equiv F_{150\mu s}$	fluorescence intensity at the L-step (150 μs) of OJIP
$F_K \equiv F_{300\mu s}$	fluorescence intensity at the K-step (300 μs) of OJIP
$F_J \equiv F_{2ms}$	fluorescence intensity at the J-step (2 ms) of OJIP
$F_I \equiv F_{30ms}$	fluorescence intensity at the I-step (30 ms) of OJIP
F_P (= F_M)	maximal recorded fluorescence intensity, at the peak P of OJIP
$F_v \equiv F_t - F_O$	variable fluorescence at time t
$F_V \equiv F_M - F_O$	maximal variable fluorescence
t_{F_M}	time (in ms) to reach the maximal fluorescence intensity F_M
$V_t \equiv (F_t - F_O)/(F_M - F_O)$	relative variable fluorescence at time t
$V_K = (F_K - F_O)/(F_M - F_O)$	relative variable fluorescence at the K-step
$V_J = (F_J - F_O)/(F_M - F_O)$	relative variable fluorescence at the J-step
$W_t \equiv (F_t - F_O)/(F_J - F_O)$	relative variable fluorescence F_V to the amplitude $F_J - F_O$
$M_0 \equiv 4(F_{270\mu s} - F_O)/(F_M - F_O)$	approximated initial slope (in ms^{-1}) of the fluorescence transient normalized on the maximal variable fluorescence F_V
$S_m \equiv Area/(F_M - F_O)$	normalized total complementary area above the O-J-I-P transient (reflecting multiple-turnover Q_A reduction events)
$S_s = V_J/M_0$	normalized total complementary area corresponding only to the O–J phase (reflecting single-turnover Q_A reduction events)
Specific energy fluxes (per Q_A-reducing PSII reaction center, RC)	
$ABS/RC = M_0 \times (1/V_J) \times (1/\varphi_{Po})$	absorption flux per RC
$TR_0/RC = M_0 \times (1/V_J)$	trapped energy flux per RC
$ET_0/RC = M_0 \times (1/V_J) \times (1 - V_J)$	electron transport flux per RC
$DI_0/RC = (ABS/RC) - (TR_0/RC)$	dissipate energy flux per RC
Quantum efficiencies or flux ratios	
$\varphi_{Po} = PHI(P_O) = TR_0/ABS = 1 - F_O/F_M$	maximum quantum yield for primary photochemistry
$\psi_{Eo} = PSI_0 = ET_0/TR_0 = (1 - V_J)$	probability that an electron moves further than Q_A^-
$\varphi_{Eo} = PHI(E_O) = ET_0/ABS = (1 - F_O/F_M)\,(1 - V_J)$	quantum yield for electron transport (ET)
$\varphi_{Do} = PHI(D_O) = 1 - \varphi_{Po} = F_O/F_M$	quantum yield (at t = 0) of energy dissipation
$\varphi_{Ro} = RE_0/ABS = \varphi_{Po} \times \psi_{Eo} \times \delta_{Ro} = \varphi_{Po} \times (1 - V_I)$	quantum yield for reduction of the end electron acceptors at the PSI acceptor side (RE)
$\delta_{Ro} = RE_0/ET_0 = (1 - V_I)/(1 - V_J)$	probability that an electron is transported from the reduced intersystem electron acceptors to the final electron acceptors of PSI
$\gamma_{RC} = Chl_{RC}/Chl_{total} = RC/(ABS + RC)$	probability that a PSII Chl molecule functions as RC

Phenomenological energy fluxes (per excited leaf cross section, CS)	
$ABS/CS_m \approx F_M$	absorption flux per excited CS, approximated by F_M
$TR_0/CS_m = \varphi_{Po} \times (ABS/CS_m)$	trapped energy flux per CS (at $t = t_{Fmax}$)
$ET_0/CS_m = \varphi_{Po} \times \psi_{Eo} \times (ABS/CS_m)$	electron transport flux per CS (at $t = t_{Fmax}$)
$DI_0/CS_m = (ABS/CS_m) – (TR_0/CS_m)$	dissipate energy flux per CS (at $t = t_{Fmax}$)
Density of RCs	
$RC/CS_m = \varphi_{Po} \times (V_J/M_0) \times (ABS/CS_m)$	Q_A-reducing RCs per CS (at $t = t_{Fmax}$)
Q_A-reducing centers $= (RC/RC_{reference})(ABS/ABS_{reference}) = [(RC/CS)_{treatment}/(RC/CS)_{control}][(ABS/CS)_{treatment}/(ABS/CS)_{control}]$	the fraction of Q_A-reducing reaction centers
Non-Q_A-reducing centers $= 1 – Q_A$-reducing centers	the fraction of non-Q_A-reducing reaction centers, also so-called heat sink centers or silent centers
OEC centers $= [1 – (V_K/V_J)]_{treatment}/[1 – (V_K/V_J)]_{control}$	the fraction of oxygen-evolving complexes (OEC) centers
$S_m/t_{Fmax} = [RC_{open}/(RC_{close} + RC_{open})]av = [Q_A/Q_{A(total)}]av$	average fraction of open RCs of PSII in the time span between 0 to t_{Fmax}
$R_J = [\psi_{Eo(control)} – \psi_{Eo(treatment)}]/\psi_{Eo(control)} = [V_{J(treatment)} – V_{J(control)}]/[1 – V_{J(control)}]$	number of PSII RCs with Q_B-site filled by PSII inhibitor
Performance indexes	
$PI_{ABS} \equiv \frac{\gamma_{RC}}{1-\gamma_{RC}} \times \frac{\varphi_{Po}}{1-\varphi_{Po}} \times \frac{\psi_{Eo}}{1-\psi_{Eo}}$	performance index (potential) for energy conservation from photons absorbed by PSII to the reduction of intersystem electron acceptors